Dynamical coupled-channels model of πN scattering in the $W \leqslant 2$ GeV nucleon resonance region

B. Juliá-Díaz,[1,2] T.-S. H. Lee,[1,3] A. Matsuyama,[1,4] and T. Sato[1,5]

[1]*Excited Baryon Analysis Center (EBAC), Thomas Jefferson National Accelerator Facility, Newport News, Virginia 22901, USA*

[2]*Departament d'Estructura i Constituents de la Matèria, Universitat de Barcelona, E–08028 Barcelona, Spain*

[3]*Physics Division, Argonne National Laboratory, Argonne, Illinois 60439, USA*

[4]*Department of Physics, Shizuoka University, Shizuoka 422-8529, Japan*

[5]*Department of Physics, Osaka University, Toyonaka, Osaka 560-0043, Japan*

(Received 3 August 2007; published 4 December 2007)

As a first step to analyze the electromagnetic meson production reactions in the nucleon resonance region, the parameters of the hadronic interactions of a dynamical coupled-channels model, developed in *Physics Reports 439, 193 (2007)*, are determined by fitting the πN-scattering data. The channels included in the calculations are πN, ηN, and $\pi\pi N$, which has $\pi\Delta$, ρN, and σN resonant components. The nonresonant meson-baryon interactions of the model are derived from a set of Lagrangians by using a unitary transformation method. One or two bare excited nucleon states in each of S, P, D, and F partial waves are included to generate the resonant amplitudes in the fits. The parameters of the model are first determined by fitting as much as possible the empirical πN elastic-scattering amplitudes of SAID up to 2 GeV. We then refine and confirm the resulting parameters by directly comparing the predicted differential cross section and target polarization asymmetry with the original data of the elastic $\pi^{\pm}p \to \pi^{\pm}p$ and charge-exchange $\pi^{-}p \to \pi^{0}n$ processes. The predicted total cross sections of πN reactions and $\pi N \to \eta N$ reactions are also in good agreement with the data. Applications of the constructed model in analyzing the electromagnetic meson production data as well as the future developments are discussed.

DOI: 10.1103/PhysRevC.76.065201 PACS number(s): 13.75.Gx, 13.60.Le, 14.20.Gk

I. INTRODUCTION

It is now well recognized that a coupled-channels approach is needed to extract the nucleon resonance (N^*) parameters from the data of πN and electromagnetic meson production reactions. With the recent experimental developments [1,2], such a theoretical effort is needed to analyze the very extensive data from Jefferson Laboratory (JLab), Mainz, Bonn, GRAAL, and Spring-8. To cope with this challenge, a dynamical coupled-channels model (Matsuyama, Sato, and Lee; MSL) for meson-baryon reactions in the nucleon resonance region has been developed recently [3]. In this article we report a first-stage determination of the parameters of this model by fitting the πN-scattering data up to invariant mass $W = 2$ GeV.

The details of the MSL model are given in Ref. [3]. Here we will only briefly recall its essential features. Similar to the earlier works on meson-exchange models [4–26] of pion-nucleon scattering, the starting point of the MSL model is a set of Lagrangians describing the interactions between mesons ($M = \gamma, \pi, \eta, \rho, \omega, \sigma, \ldots$) and baryons ($B = N, \Delta, N^*, \ldots$). By applying a unitary transformation method [13,27], an effective Hamiltonian is then derived from the considered Lagrangian. It can be cast into the following more transparent form

$$H_{\rm eff} = H_0 + \Gamma_V + v_{22} + h_{\pi\pi N}, \tag{1}$$

where $H_0 = \sum_\alpha \sqrt{m_\alpha^2 + \vec{p}_\alpha^{\,2}}$ with m_α denoting the mass of particle α, and

$$\Gamma_V = \left\{ \sum_{N^*} \left(\sum_{MB} \Gamma_{N^* \to MB} \right) + \sum_{M^*} h_{M^* \to \pi\pi} \right\} + \{c.c.\}, \tag{2}$$

$$v_{22} = \sum_{MB, M'B'} v_{MB, M'B'} + v_{\pi\pi}, \tag{3}$$

$$h_{\pi\pi N} = \sum_{N^*} \Gamma_{N^* \to \pi\pi N} + \sum_{MB} [(v_{MB, \pi\pi N}) + (c.c.)] + v_{\pi\pi N, \pi\pi N}. \tag{4}$$

Here $c.c.$ denotes the complex conjugate of the terms on its left-hand side. In the above equations, $MB = \gamma N, \pi N, \eta N, \pi\Delta, \rho N, \sigma N$, represent the considered meson-baryon states. The resonance associated with the *bare* baryon state N^* is induced by the vertex interactions $\Gamma_{N^* \to MB}$ and $\Gamma_{N^* \to \pi\pi N}$. Similarly, the *bare* meson states $M^* = \rho, \sigma$ can develop into resonances through the vertex interaction $h_{M^* \to \pi\pi}$. Note that the masses $M^0_{N^*}$ and $m^0_{M^*}$ of the bare states N^* and M^* are the parameters of the model that must be determined by fitting the πN- and $\pi\pi$-scattering data. They differ from the empirically determined resonance positions by mass shifts that are due to the coupling of the bare states to the scattering states. The term v_{22} contains the nonresonant meson-baryon interaction $v_{MB, M'B'}$ and $\pi\pi$ interaction $v_{\pi\pi}$. The nonresonant interactions involving $\pi\pi N$ states are in $h_{\pi\pi N}$. All of these interactions are *energy independent*, an important feature of the MSL formulation.

We note here that the Hamiltonian defined above does not have a $\pi N \leftrightarrow N$ vertex. By applying the unitary transformation method, this unphysical process as well as any vertex interaction $A \leftrightarrow B + C$ with a mass relation $m_A < m_B + m_C$ are eliminated from the considered Hilbert space and their effects are absorbed in the effective interactions v_{22} and $h_{\pi\pi N}$. This procedure defines the Hamiltonian in terms of physical nucleons and greatly simplifies the formulation of a unitary

reaction model. In particular, the complications due to the nucleon mass and wave function renormalizations do not appear in the resulting scattering equations. This makes the numerical calculations involving the $\pi\pi N$ channel much more tractable in practice. The details of this approach are discussed in Refs. [13,27] as well as in the earlier works on πNN interactions [28].

Starting from the above Hamiltonian, the coupled-channels equations for πN and γN reactions are then derived by using the standard projection operator technique [29], as given explicitly in Ref. [3]. The obtained scattering equations satisfy the two-body (πN, ηN, γN) and three-body ($\pi\pi N$) unitarity conditions. The $\pi\Delta$, ρN, and σN resonant components of the $\pi\pi N$ continuum are generated dynamically by the vertex interaction Γ_V of Eq. (2). Accordingly, the $\pi\pi N$ cuts are treated more rigorously than the commonly used quasiparticle formulation within which these resonant channels are treated as simple two-particle states with a phenomenological parametrization of their widths. The importance of such a dynamical treatment of unstable particle channels was well known in earlier studies of πN scattering [4,30] and πNN reactions [31].

A complete determination of the parameters of the model Hamiltonian defined by Eqs. (1)–(4) requires good fits to all of the data of πN and γN reactions up to invariant mass $W \leqslant$ about 2 GeV. Obviously, this is a very complex task and can be accomplished only step by step. Our strategy is as follows. We need to first determine the parameters associated with the hadronic interaction parts of the Hamiltonian. With the fits to $\pi\pi$ phase shifts in Ref. [32], the $\pi\pi$ interactions $h_{\rho,\pi\pi}$ and $h_{\sigma,\pi\pi}$ and the corresponding bare masses for ρ and σ have been determined in an isobar model with $v_{\pi\pi} = 0$. We next proceed in two stages. The first stage is to determine the ranges of the parameters of the interactions $\Gamma_{N^*\to MB}$ and $v_{MB,M'B'}$. This will be achieved by fitting the πN-scattering data from performing coupled-channels calculations which neglect the more complex three-body interaction term $h_{\pi\pi N}$. This simplification greatly reduces the numerical complexity and the number of parameters to be determined in the fits. This first-stage fit will provide the starting parameters to fit both the data of πN scattering and $\pi N \to \pi\pi N$ reactions. In this second-stage, the parameters associated with $\Gamma_{N^*\to MB}$ and $v_{MB,M'B'}$ will be refined and the parameters of $h_{\pi\pi N}$ are then determined. The dynamical coupled-channels calculations for such more extensive fits are numerically more complex, as explained in Ref. [3].

In this work we report on the results from our first-stage determination of the parameters of $\Gamma_{N^*\to MB}$ and $v_{MB,M'B'}$ of Eqs. (2)–(3) with $MB, M'B' = \pi N, \eta N, \pi\Delta, \rho N, \sigma N$. We proceed in two steps. We first locate the range of the model parameters by fitting as much as possible the empirical πN elastic-scattering amplitudes up to $W = 2$ GeV of SAID [33]. We then refine and confirm the resulting parameters by directly comparing our predictions with the original πN-scattering data. Our procedures are similar to what have been used in determining the nucleon-nucleon (NN) potentials [34] from fitting NN-scattering data.

The constructed model can describe well almost all of the empirical πN amplitudes in S, P, D, and F partial waves of SAID [33]. We then show that the predicted differential cross sections and target polarization asymmetry are in good agreement with the original data of elastic $\pi^\pm p \to \pi^\pm p$ and charge-exchange $\pi^- p \to \pi^0 n$ processes. Furthermore the predicted total cross sections of the πN reactions and $\pi N \to \eta N$ reactions agree well with the data. Thus the constructed model is at least comparable to, if not better than, all of the recent πN models [11–13,19,20,22–24,26]. It can be used to perform a first-stage extraction of the $\gamma N \to N^*$ parameters by analyzing the photo- and electroproduction of *single* π meson. It has also provided us with a starting point for performing the second-stage determination of the model parameters by also fitting the data of $\pi N \to \pi\pi N$ reactions. Our efforts in these directions are in progress and will be reported elsewhere.

In Sec. II, we recall the coupled-channels equations presented in Ref. [3]. The calculations performed in this work are described in Sec. III. The fitting procedure is described in Sec. IV and the results are presented in Sec. V. In Sec. VI we give a summary and discuss future developments.

II. DYNAMICAL COUPLED-CHANNELS EQUATIONS

With the simplification that $\pi\pi N$ interaction $h_{\pi\pi N}$ of Eq. (4) is set to zero, the meson-baryon (MB) scattering equations derived in Ref. [3] are illustrated in Fig. 1. Explicitly, they are defined by the following equations

$$T_{MB,M'B'}(E) = t_{MB,M'B'}(E) + t^R_{MB,M'B'}(E), \tag{5}$$

where $MB = \pi N, \eta N, \pi\Delta, \rho N, \sigma N$. The full amplitudes $T_{\pi N,\pi N}(E)$ can be directly used to calculate πN-scattering observables. The nonresonant amplitude $t_{MB,M'B'}(E)$ in Eq. (5) is defined by the coupled-channels equations,

$$t_{MB,M'B'}(E) = V_{MB,M'B'}(E) + \sum_{M''B''} V_{MB,M''B''}(E)\, G_{M''B''}(E) \times t_{M''B'',M'B'}(E) \tag{6}$$

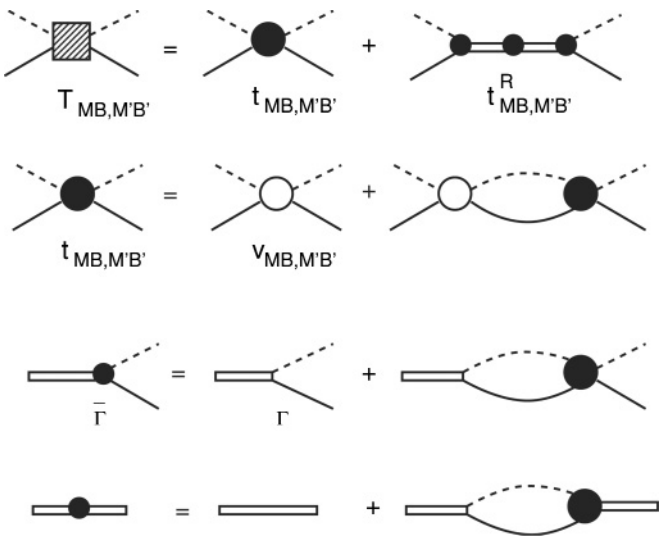

FIG. 1. Graphical representation of Eqs. (5)–(21).

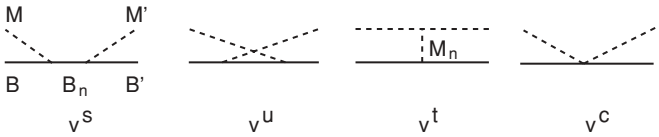

FIG. 2. Mechanisms for $v_{MB,M'B'}$ of Eq. (7): v^s direct s channel, v^u crossed u channel, v^t one-particle-exchange t channel, v^c contact interactions.

with

$$V_{MB,M'B'}(E) = v_{MB,M'B'} + Z^{(E)}_{MB,M'B'}(E). \tag{7}$$

Here the interactions $v_{MB,M'B'}$ are derived from the tree-diagrams illustrated in Fig. 2 by using a unitary transformation method [13,27]. It is energy independent and free of singularity. However, $Z^{(E)}_{MB,M'B'}(E)$ is induced by the decays of the unstable particles (Δ, ρ, σ) and thus contains *moving* singularities due to the $\pi\pi N$ cuts, as illustrated in Fig. 3. Here we note that if the $\pi\pi N$ interaction term $h_{\pi\pi N}$ of Eq. (4) is included, the driving term Eq. (7) will have an additional term $Z^{(I)}_{MB,M'B'}(E)$ that involves a 3–3 $\pi\pi N$ amplitude $t_{\pi\pi N,\pi\pi N}$, as given in Ref. [3] and hence is much more difficult to calculate. As explained in Sec. I, we neglect this term in this first-stage fit to the πN-scattering data.

The second term in the right-hand side of Eq. (5) is the resonant term defined by

$$t^R_{MB,M'B'}(E) = \sum_{N^*_i,N^*_j} \bar{\Gamma}_{MB\to N^*_i}(E)[D(E)]_{i,j}\bar{\Gamma}_{N^*_j\to M'B'}(E), \tag{8}$$

with

$$[D^{-1}(E)]_{i,j} = \left(E - M^0_{N^*_i}\right)\delta_{i,j} - \bar{\Sigma}_{i,j}(E), \tag{9}$$

where $M^0_{N^*}$ is the bare mass of the resonant state N^* and the self-energies are

$$\bar{\Sigma}_{i,j}(E) = \sum_{MB} \Gamma_{N^*_i\to MB}G_{MB}(E)\bar{\Gamma}_{MB\to N^*_j}(E). \tag{10}$$

The dressed vertex interactions in Eq. (8) and Eq. (10) are (defining $\Gamma_{MB\to N^*} = \Gamma^\dagger_{N^*\to MB}$)

$$\bar{\Gamma}_{MB\to N^*}(E) = \Gamma_{MB\to N^*} + \sum_{M'B'} t_{MB,M'B'}(E) \times G_{M'B'}(E)\Gamma_{M'B'\to N^*}, \tag{11}$$

$$\bar{\Gamma}_{N^*\to MB}(E) = \Gamma_{N^*\to MB} + \sum_{M'B'} \Gamma_{N^*\to M'B'} \times G_{M'B'}(E)t_{M'B',MB}(E). \tag{12}$$

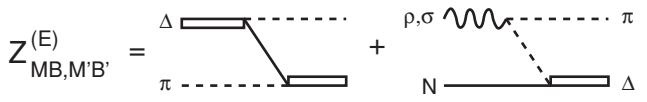

FIG. 3. One-particle-exchange interactions $Z^{(E)}_{\pi\Delta,\pi\Delta}(E)$, $Z^{(E)}_{\rho N,\pi\Delta}$, and $Z^{(E)}_{\sigma N,\pi\Delta}$ of Eq. (7).

It is useful to mention here that if there is only one N^* in the considered partial wave, the resonant amplitude [Eq. (8)] can be written as

$$t^R_{MB,M'B'}(E) = \frac{\bar{\Gamma}_{MB\to N^*_1}(E)\bar{\Gamma}_{N^*_1\to M'B'}(E)}{E - E_R(E) + i\frac{\Gamma_R(E)}{2}} \tag{13}$$

with

$$E_R(E) = M^0_{N^*} + \mathrm{Re}[\bar{\Sigma}(E)], \tag{14}$$

$$\Gamma_R(E) = -2\mathrm{Im}[\bar{\Sigma}(E)], \tag{15}$$

where

$$\bar{\Sigma}(E) = \sum_{MB}\Gamma_{N^*\to MB}G_{MB}(E)\Big\{\sum_{M'B'}[\delta_{MB,M'B'} + t_{MB,M'B'}(E)G_{M'B'}(E)]\Big\}\Gamma_{M'B'\to N^*}(E). \tag{16}$$

The form Eq. (13) is similar to the commonly used Breit-Wigner form, but the resonance position $E_R(E)$ and width $\Gamma_R(E)$ are determined by the $N^* \to MB$ vertex and the nonresonant amplitude $t_{MB,M'B'}$. This is the consequence of the unitarity condition and is an important and well-known feature of a dynamical approach. Namely the resonance amplitude necessarily includes the nonresonant mechanisms. This feature is consistent with the well-developed formal reaction theory [29]. Equation (16) indicates that it is essential to understand the nonresonant mechanisms in extracting the bare vertex functions $\Gamma_{N^*,MB}$ that contain the information for exploring the N^* structure. The parametrization used for $\Gamma_{N^*,MB}$ will be explained in Sec. III. We also note here that the energy dependence of $E_R(E)$ and $\Gamma_R(E)$, defined by Eqs. (14)–(15), is essential in determining the resonance poles in the complex E-plane.

The meson-baryon propagators G_{MB} in the above equations are

$$G_{MB}(k, E) = \frac{1}{E - E_M(k) - E_B(k) + i\epsilon} \tag{17}$$

for the stable particle channels $MB = \pi N, \eta N$, and

$$G_{MB}(k, E) = \frac{1}{E - E_M(k) - E_B(k) - \Sigma_{MB}(k, E)} \tag{18}$$

for the unstable particle channels $MB = \pi\Delta, \rho N, \sigma N$. The self-energies [35] in Eq. (18) are

$$\Sigma_{\pi\Delta}(k, E) = \frac{m_\Delta}{E_\Delta(k)}\int q^2dq\frac{M_{\pi N}(q)}{\left[M^2_{\pi N}(q) + k^2\right]^{1/2}}\frac{|f_{\Delta,\pi N}(q)|^2}{E - E_\pi(k) - \{[E_N(q) + E_\pi(q)]^2 + k^2\}^{1/2} + i\epsilon}, \tag{19}$$

$$\Sigma_{\rho N}(k, E) = \frac{m_\rho}{E_\rho(k)}\int q^2dq\frac{M_{\pi\pi}(q)}{\left[M^2_{\pi\pi}(q) + k^2\right]^{1/2}}\frac{|f_{\rho,\pi\pi}(q)|^2}{E - E_N(k) - \{[2E_\pi(q)]^2 + k^2\}^{1/2} + i\epsilon}, \tag{20}$$

$$\Sigma_{\sigma N}(k, E) = \frac{m_\sigma}{E_\sigma(k)} \int q^2 dq \frac{M_{\pi\pi}(q)}{\left[M^2_{\pi\pi}(q) + k^2\right]^{1/2}} \frac{|f_{\sigma,\pi\pi}(q)|^2}{E - E_N(k) - \{[2E_\pi(q)]^2 + k^2\}^{1/2} + i\epsilon}, \tag{21}$$

where $M_{\pi N}(q) = E_\pi(q) + E_N(q)$ and $M_{\pi\pi}(q) = 2E_\pi(q)$. The vertex function $f_{\Delta,\pi N}(q)$ is taken from Ref. [13], $f_{\rho,\pi\pi}(q)$ and $f_{\sigma,\pi\pi}(q)$ are from the isobar fits [32] to the $\pi\pi$ phase shifts. They are also given explicitly in Ref. [3].

Here we note that the driving term $Z^{(E)}_{MB,M'B'}$ of Eq. (7) is also determined by the same vertex functions $f_{\Delta,\pi N}(q)$, $f_{\rho,\pi\pi}(q)$, and $f_{\rho,\pi\pi}(q)$ of Eqs. (19)–(21). This consistency is essential for the solutions of Eq. (6) to satisfy the unitarity condition.

III. CALCULATIONS

We solve the coupled-channels equations defined by Eqs. (5)–(21) in the partial-wave representation. The input of these equations are the partial-wave matrix elements of $\Gamma_{N^*\to MB}$ and $v_{MB,M'B'}$ of Eqs. (2)–(3), with $MB, M'B' = \pi N, \eta N, \pi\Delta, \rho N, \sigma N$, and $Z^{(E)}_{MB,M'B'}$ of Eq. (7) with $MB, M'B' = \pi\Delta, \rho N, \sigma N$. The calculations of these matrix elements have been given explicitly in the appendices of Ref. [3]. Here we only mention a few points that are needed for later discussions.

In deriving the nonresonant interactions $v_{MB,M'B'}$ of Eq. (7) we consider the tree-diagrams (Fig. 2) generated from a set of Lagrangians with $\pi, \eta, \sigma, \rho, \omega, N$, and Δ fields. The higher mass mesons, such as a_0, a_1 included in other meson-exchange πN models, such as the Jülich model [19], are not considered. The employed Lagrangians are (in the convention of Bjorken and Drell [36])

$$L_{\pi NN} = -\frac{f_{\pi NN}}{m_\pi} \bar\psi_N \gamma_\mu \gamma_5 \vec\tau \psi_N \cdot \partial^\mu \vec\phi_\pi, \tag{22}$$

$$L_{\pi N\Delta} = -\frac{f_{\pi N\Delta}}{m_\pi} \bar\psi^\mu_\Delta \vec T \psi_N \cdot \partial_\mu \vec\phi_\pi, \tag{23}$$

$$L_{\pi\Delta\Delta} = \frac{f_{\pi\Delta\Delta}}{m_\pi} \bar\psi_{\Delta\mu} \gamma^\nu \gamma_5 \vec T_\Delta \psi^\mu_\Delta \cdot \partial_\nu \vec\phi_\pi, \tag{24}$$

$$L_{\eta NN} = -\frac{f_{\eta NN}}{m_\eta} \bar\psi_N \gamma_\mu \gamma_5 \psi_N \partial^\mu \phi_\eta. \tag{25}$$

$$L_{\rho NN} = g_{\rho NN} \bar\psi_N \left(\gamma_\mu - \frac{\kappa_\rho}{2m_N} \sigma_{\mu\nu} \partial^\nu\right) \vec\rho^\mu \cdot \frac{\vec\tau}{2} \psi_N, \tag{26}$$

$$L_{\rho N\Delta} = -i \frac{f_{\rho N\Delta}}{m_\rho} \bar\psi^\mu_\Delta \gamma^\nu \gamma_5 \vec T \cdot (\partial_\mu \vec\rho_\nu - \partial_\nu \vec\rho_\mu) \psi_N + (h.c.), \tag{27}$$

$$L_{\rho\Delta\Delta} = g_{\rho\Delta\Delta} \bar\psi_{\Delta\alpha} \left(\gamma^\mu - \frac{\kappa_{\rho\Delta\Delta}}{2m_\Delta} \sigma^{\mu\nu} \partial_\nu\right) \vec\rho_\mu \cdot \vec T_\Delta \psi^\alpha_\Delta, \tag{28}$$

$$L_{\rho\pi\pi} = g_{\rho\pi\pi} (\vec\phi_\pi \times \partial_\mu \vec\phi_\pi) \cdot \vec\rho^\mu, \tag{29}$$

$$L_{NN\rho\pi} = \frac{f_{\pi NN}}{m_\pi} g_{\rho NN} \bar\psi_N \gamma_\mu \gamma_5 \vec\tau \psi_N \cdot \vec\rho^\mu \times \vec\phi_\pi, \tag{30}$$

$$L_{NN\rho\rho} = -\frac{\kappa_\rho g^2_{\rho NN}}{8m_N} \bar\psi_N \sigma^{\mu\nu} \vec\tau \psi_N \cdot \vec\rho_\mu \times \vec\rho_\nu. \tag{31}$$

$$L_{\omega NN} = g_{\omega NN} \bar\psi_N \left(\gamma_\mu - \frac{\kappa_\omega}{2m_N} \sigma_{\mu\nu} \partial^\nu\right) \omega^\mu \psi_N, \tag{32}$$

$$L_{\omega\pi\rho} = -\frac{g_{\omega\pi\rho}}{m_\omega} \epsilon_{\mu\alpha\lambda\nu} \partial^\alpha \vec\rho^\mu \cdot \partial^\lambda \vec\phi_\pi \omega^\nu, \tag{33}$$

$$L_{\sigma NN} = g_{\sigma NN} \bar\psi_N \psi_N \phi_\sigma \tag{34}$$

$$L_{\sigma\pi\pi} = -\frac{g_{\sigma\pi\pi}}{2m_\pi} \partial^\mu \vec\varphi_\pi \cdot \partial_\mu \vec\varphi_\pi \phi_\sigma. \tag{35}$$

To solve the coupled-channels equations, Eq. (6), we need to regularize the matrix elements of $v_{MB,M'B'}$, illustrated in Fig. 2. Here we follow Ref. [13] to use the parameters determined in the Δ (1232) region as the starting parameters in our fits. For the v^s and v^u terms of Fig. 2, we include at each meson-baryon-baryon vertex a form factor of the following form

$$F(\vec k, \Lambda) = [\vec k^2/(\vec k^2 + \Lambda^2)]^2 \tag{36}$$

with $\vec k$ being the meson momentum. For the meson-meson-meson vertex of v^t of Fig. 2, the form Eq. (36) is also used with $\vec k$ being the momentum of the exchanged meson. For the contact term v^c, we regularize it by $F(\vec k, \Lambda) F(\vec k', \Lambda')$.

With the nonresonant amplitudes generated from solving Eq. (6), the resonant amplitude $t^R_{MB,M'B'}$ Eq. (8) then depends on the bare mass $M^0_{N^*}$ and the bare $N^* \to MB$ vertex functions. As discussed in Ref. [3], these bare N^* parameters can perhaps be taken from a hadron structure calculation

TABLE I. The orbital angular momentum (L) and total spin (S) of the partial waves included in solving the coupled-channels equation [Eq. (6)].

	(LS) of the considered partial waves				
	πN	ηN	$\pi\Delta$	σN	ρN
S_{11}	$(0, \frac{1}{2})$	$(0, \frac{1}{2})$	$(2, \frac{3}{2})$	$(1, \frac{1}{2})$	$(0, \frac{1}{2}), (2, \frac{3}{2})$
S_{31}	$(0, \frac{1}{2})$	–	$(2, \frac{3}{2})$	–	$(0, \frac{1}{2}), (2, \frac{3}{2})$
P_{11}	$(1, \frac{1}{2})$	$(1, \frac{1}{2})$	$(1, \frac{3}{2})$	$(0, \frac{1}{2})$	$(1, \frac{1}{2}), (1, \frac{3}{2})$
P_{13}	$(1, \frac{1}{2})$	$(1, \frac{1}{2})$	$(1, \frac{3}{2}), (3, \frac{3}{2})$	$(2, \frac{1}{2})$	$(1, \frac{1}{2}), (1, \frac{3}{2}), (3, \frac{3}{2})$
P_{31}	$(1, \frac{1}{2})$	–	$(1, \frac{3}{2})$	–	$(1, \frac{1}{2}), (1, \frac{3}{2})$
P_{33}	$(1, \frac{1}{2})$	–	$(1, \frac{3}{2}), (3, \frac{3}{2})$	–	$(1, \frac{1}{2}), (1, \frac{3}{2}), (3, \frac{3}{2})$
D_{13}	$(2, \frac{1}{2})$	$(2, \frac{1}{2})$	$(0, \frac{3}{2}), (2, \frac{3}{2})$	$(1, \frac{1}{2})$	$(2, \frac{1}{2}), (0, \frac{3}{2}), (4, \frac{3}{2})$
D_{15}	$(2, \frac{1}{2})$	$(2, \frac{1}{2})$	$(2, \frac{3}{2}), (4, \frac{3}{2})$	$(3, \frac{1}{2})$	$(2, \frac{1}{2}), (2, \frac{3}{2}), (4, \frac{3}{2})$
D_{33}	$(2, \frac{1}{2})$	–	$(0, \frac{3}{2}), (2, \frac{3}{2})$	–	$(2, \frac{1}{2}), (0, \frac{3}{2}), (2, \frac{3}{2})$
D_{35}	$(2, \frac{1}{2})$	–	$(2, \frac{3}{2}), (4, \frac{3}{2})$	–	$(2, \frac{1}{2}), (2, \frac{3}{2}), (4, \frac{3}{2})$
F_{15}	$(3, \frac{1}{2})$	$(3, \frac{1}{2})$	$(1, \frac{3}{2}), (3, \frac{3}{2})$	$(2, \frac{1}{2})$	$(3, \frac{1}{2}), (1, \frac{3}{2}), (3, \frac{3}{2})$
F_{17}	$(3, \frac{1}{2})$	$(3, \frac{1}{2})$	$(3, \frac{3}{2}), (5, \frac{3}{2})$	$(4, \frac{1}{2})$	$(3, \frac{1}{2}), (3, \frac{3}{2}), (5, \frac{1}{2})$
F_{35}	$(3, \frac{1}{2})$	–	$(1, \frac{3}{2}), (3, \frac{3}{2})$	–	$(3, \frac{1}{2}), (1, \frac{3}{2}), (3, \frac{3}{2})$
F_{37}	$(3, \frac{1}{2})$	–	$(3, \frac{3}{2}), (5, \frac{3}{2})$	–	$(3, \frac{1}{2}), (3, \frac{3}{2}), (5, \frac{3}{2})$

that *does not* include coupling with meson-baryon continuum states or meson-exchange quark interactions. Unfortunately, such information is not available to us. We thus use the following parametrization

$$\Gamma_{N^*,MB(LS)}(k) = \frac{1}{(2\pi)^{3/2}}\frac{1}{\sqrt{m_N}} C_{N^*,MB(LS)} \times \left[\frac{\Lambda^2_{N^*,MB(LS)}}{\Lambda^2_{N^*,MB(LS)} + (k-k_R)^2}\right]^{(2+L)} \left[\frac{k}{m_\pi}\right]^L, \tag{37}$$

where L and S are the orbital angular momentum and the total spin of the MB system, respectively. The above parametrization accounts for the threshold k^L dependence and the right power $(2+L)$ such that the integration for calculating the dressed vertex Eq. (11)–(12) is finite. Nevertheless as we will discuss in Sec. V this parametrization could be too naive. We mention here that the normalization of the vertex function defined by Eq. (37) is chosen to give the

$$\text{partial decay width} = \frac{2\pi}{(2J_{N^*}+1)} |\Gamma_{N^*,MB(LS)}(k)|^2 \times \frac{kE_B(k)E_M(k)}{W}, \tag{38}$$

with $W = E_B(k) + E_M(k)$.

The partial-wave quantum numbers for the considered channels are listed in Table I. The numerical methods for handling the moving singularities due to the $\pi\pi N$ cuts in $Z^{(E)}_{MB,M'B'}$ (Fig. 3) in solving Eq. (6) are explained in detail in Ref [3]. To get the πN elastic-scattering amplitudes, we can use either the method of contour rotation by solving the equations on the complex momentum axis $k = ke^{-i\theta}$ with $\theta > 0$ or the spline-function method developed in Refs. [37,38] and explained in detail in Ref. [3]. We perform the calculations using these two very different methods and they agree within less than 1%. When $Z^{(E)}_{MB,M'B'}$ is neglected, Eq. (6) can be solved by the standard subtraction method because the resonant propagators, Eqs. (18), for unstable particle channels $\pi\Delta$, ρN, and σN are free of singularity on the real momentum axis. A code for this simplified case has also been developed to confirm the results from using the other two methods.

The method of contour rotation becomes difficult at high W because the required rotation angle θ is very small. The spline function method has no such limitation and we can perform calculations at $W > 1.9$ GeV without any difficulty. Typically, 24 and 32 mesh points are needed to get convergent solutions of the coupled-channels integral equation (6). Such mesh points are also needed to get stable integrations in evaluating the dressed resonance quantities Eqs. (10)–(12).

IV. FITTING PROCEDURE

With the specifications given in Sec. III, the parameters associated with $Z^{(E)}_{MB,M'B'}$ of Eq. (7) are completely determined from fitting the $\pi\pi$ phase shifts in Refs. [13] and [32]. Thus the considered model has the following parameters: (a) the coupling constants associated with the Lagrangians listed in Eqs. (22)–(34), (b) the cutoff Λ for each vertex of $v_{MB,M'B'}$ (Fig. 2), (c) the coupling strength $C_{N^*,MB(LS)}$ and range k_R and $\Lambda_{N^*,MB(LS)}$ of the bare $N^* \to MB$ vertex Eq. (37), and (d) the bare mass $M^0_{N^*}$ of each N^* state. We determine these by fitting the πN-scattering data.

Our fitting procedure is as follows. We first perform fits to the πN-scattering data up to about 1.4 GeV and including only one bare state, the Δ (1232) resonance. In these fits, the starting coupling constant parameters of $v_{MB,M'B'}$ are taken from the previous studies of πN and NN scattering, which are also given in Ref. [3]. Except the πNN coupling constant $f_{\pi NN}$ all coupling constants and the cutoff parameters are allowed to vary in the χ^2-fit to the πN data. The coupled-channels effects can shift the coupling constants greatly from their starting values. We try to minimize these shifts by allowing the cutoff parameters to vary in a very wide range 500 MeV $< \Lambda <$ 2000 MeV. Some signs of coupling constants, which could not be fixed by the previous works [39], are also allowed to change. We then use the parameters from these fits at low energies as the starting ones to fit the amplitudes up to 2 GeV by also adjusting the resonance parameters, $M^0_{N^*}$, $C_{N^*,MB(LS)}$, k_R and $\Lambda_{N^*,MB(LS)}$. Here we need to specify the number of bare N^* states in each partial wave. The simplest approach is to assume that each of three-star and four-star resonances listed by the Particle Data Group [40] is generated from a bare N^* state of the model Hamiltonian Eq. (1). However, this choice is perhaps not well justified because the situation of the higher mass N^*'s is not so clear.

We thus start the fits including only the bare states that generate the *lowest* and well-established N^* resonance in each partial wave. The second higher mass bare state is then included when a good fit cannot be achieved. We also impose the condition that if the resulting $M^0_{N^*}$ is too high >2.5 GeV, we remove such a bare state in the fit. This is due to the consideration that the interactions due to such a heavy bare N^* state could be just the separable representation of some nonresonant mechanisms that should be included in $v_{MB,M'B'}$. In some partial waves the quality of the fits is not very sensitive to the N^* couplings to $\pi\Delta$, ρN, and σN. But the freedom of varying these coupling parameters is needed to achieve good fits.

It is rather difficult to fit all partial waves simultaneously because the number of resonance parameters to be determined is very large. We proceed as follows. We first fit only three or four partial waves that have well-established resonant states and whose amplitudes have an involved energy dependence. These are the S_{11}, P_{11}, S_{31}, and P_{33} partial waves. These fits are aimed at identifying the possible ranges of the parameters associated with $v_{MB,M'B'}$. This step is most difficult and time-consuming. We then gradually extend the fits to include more partial waves. For some cases, the fits can be reached easily by simply adjusting the bare N^* parameters. But it often requires some adjustments of the nonresonance parameters to obtain new fits. This procedure has to be repeated many times to explore the parameter space as much as we can. We carry out this very involved numerical task by using the fitting code MINUIT and the parallel computation facilities at NERSC in the United States and the Barcelona Supercomputing Center in Spain.

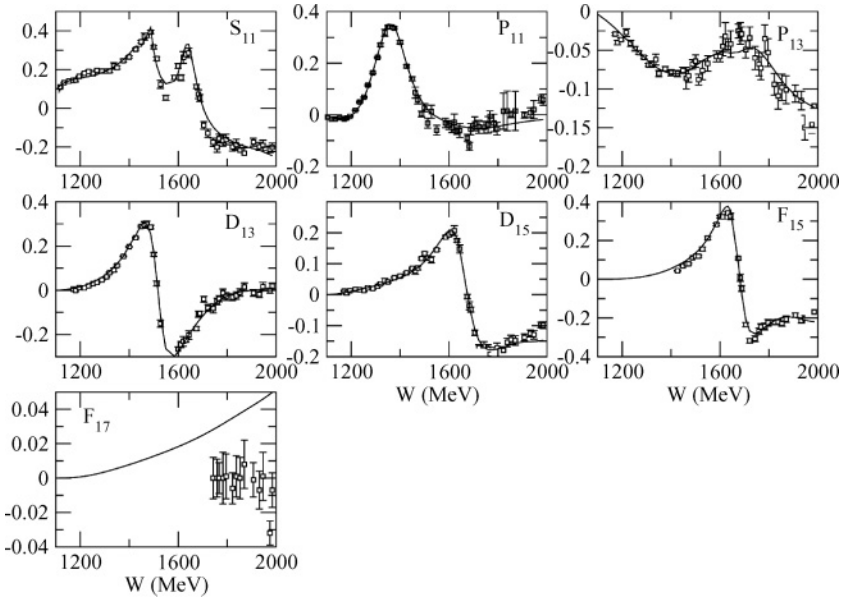

FIG. 4. Real parts of the calculated πN partial-wave amplitudes [Eq. (5)] of isospin $T = 1/2$ are compared with the energy independent solutions of Ref. [33].

The most uncertain part of the fitting is to handle the large number of parameters associated with the bare N^* states. Here the use of the empirical partial-wave amplitudes from SAID is an essential step in the fit. It allows us to locate the ranges of the N^* parameters partial wave by partial wave for a given set of the parameters for the nonresonant $v_{MB,M'B'}$. Even with this, the information is far from complete for pinning down the N^* parameters. Perhaps the N^* parameters associated with the πN state are reasonably well determined in this fit to the πN-scattering data. The parameters associated with ηN, $\pi\Delta$, ρN, and σN can only be better determined by also fitting to the data of $\pi N \to \eta N$ and $\pi N \to \pi\pi N$ reactions. This will be pursued in our second-stage calculations, as discussed in Sec. I.

It is useful to note here that the leading-order effect due to $Z^{(E)}$ of the meson-baryon interaction Eq. (7) on πN elastic scattering is

$$\delta v_{\pi N,\pi N} = \sum_{MB,M'B'=\pi\Delta,\rho N,\sigma N} v_{\pi N,MB} G_{MB}(E) Z^{(E)}_{MB,M'B'} \times G_{M'B'}(E) v_{M'B',\pi N}. \quad (39)$$

We have found by explicit numerical calculations that $\delta v_{\pi N,\pi N}$ is much weaker than $v_{\pi N,\pi N}$ and hence the coupled channel effects due to $Z^{(E)}_{MB,M'B'}$ on πN elastic-scattering amplitude are weak. One example obtained from our model is shown in Table II. Thus we first perform the fits without including $Z^{(E)}$ term to speed up the computation. We then refine the parameters by including this term in the fits.

TABLE II. The effect of $Z^{(E)}_{MB,M'B'}$ on the πN-scattering amplitudes $t_{\pi N,\pi N}$ from solving Eq. (6) at $W = 1.7$ GeV. The normalization is $t_{\pi N,\pi N} = (e^{2i\delta_{\pi N}} - 1)/(2i)$, where $\delta_{\pi N}$ is the πN-scattering phase shift that could be complex at energies above the π production threshold.

	$\mathrm{Re}(t_{\pi N,\pi N})$	$\mathrm{Re}[t_{\pi N,\pi N}(Z^{(E)}=0)]$	$\mathrm{Im}(t_{\pi N,\pi N})$	$\mathrm{Im}[t_{\pi N,\pi N}(Z^{(E)}=0)]$
S_{11}	−0.00481	−0.00557	0.0841	0.0827
P_{11}	0.0937	0.103	0.636	0.640
P_{13}	0.169	0.181	0.275	0.275
D_{13}	0.202	0.194	0.299	0.309
D_{15}	0.117	0.116	0.0179	0.0179
F_{15}	0.290	0.291	0.157	0.155
F_{17}	0.0360	0.0359	0.00293	0.00289
S_{31}	−0.433	−0.437	0.496	0.504
P_{31}	−0.253	−0.230	0.434	0.448
P_{33}	0.0506	0.0306	0.510	0.457
D_{33}	−0.00504	−0.0135	0.106	0.104
D_{35}	0.0551	0.0551	0.0540	0.0537
F_{35}	−0.0214	−0.0229	0.0259	0.0283
F_{37}	0.0625	0.0626	0.00502	0.00512

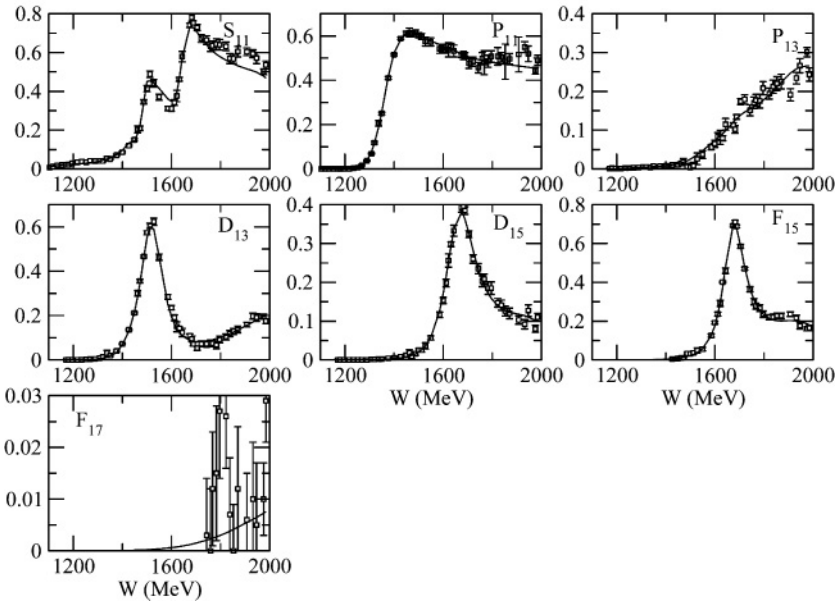

FIG. 5. Imaginary parts of the calculated πN partial wave amplitudes [Eq. (5)] of isospin $T = 1/2$ are compared with the energy independent solutions of Ref. [33].

V. RESULTS

As mentioned in Sec. I, we first locate the range of the parameters by fitting the empirical πN-scattering amplitude of SAID [33]. We then check and refine the resulting parameters by directly comparing our predictions with the original πN-scattering data.

Our fits to the empirical amplitudes of SAID [33] are given in Figs. 4–5 and Figs. 6–7 for the $T = 1/2$ and $T = 3/2$ partial waves, respectively. The resulting parameters are presented in Appendix. The parameters associated with the nonresonant interactions, $v_{MB,M'B'}$ with $MB, M'B' = \pi N, \eta N, \pi\Delta, \rho N, \sigma N$, are given in Table III for the coupling constants of the starting Lagrangian Eqs. (22)–(34) and Table IV for the cutoffs of the form factors defined by Eq. (36). The resulting bare N^* parameters are listed in Tables V–VII.

From Figs. 4–7, one can see that the empirical πN amplitudes can be fitted very well. The most significant discrepancies are in the imaginary part of S_{31} in Fig. 7. The agreement is also poor for the F_{17} in Figs. 4–5 and D_{35} in Figs. 6–7, but there are rather large errors in the data. Our parameters are therefore checked by directly comparing our predictions with the data of differential cross sections $d\sigma/d\Omega$ and target polarization asymmetry P of elastic $\pi^{\pm}p \to \pi^{\pm}p$ and charge-exchange $\pi^{-}p \to \pi^{0}n$ processes. Our results (solid red curves) are shown in Figs. 8–12. Clearly, our model is rather consistent with the available data and are close to the results (dashed blue curves) calculated from the SAID's amplitudes. Thus our model is justified despite the differences with the SAID's amplitudes seen in Figs. 4–7.

It will be important to further refine our parameters by fitting the data of other πN-scattering observables, such as the recoil polarization and double polarization. Hopefully, such

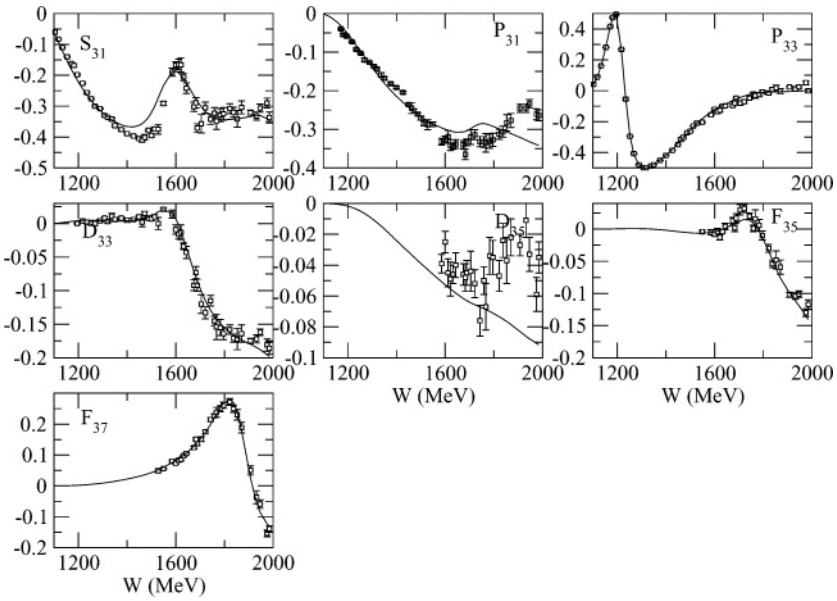

FIG. 6. Real parts of the calculated πN partial-wave amplitudes [Eq. (5)] of isospin $T = 3/2$ are compared with the energy independent solutions of Ref. [33].

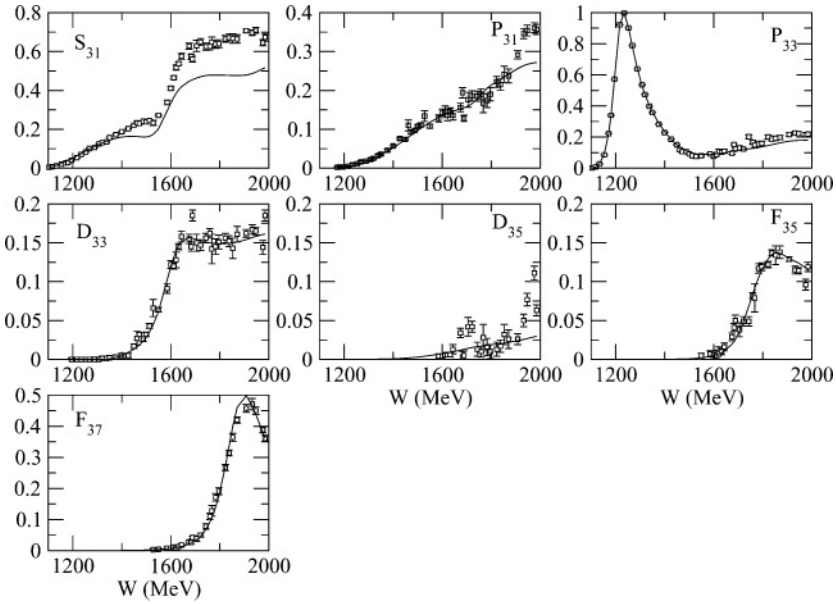

FIG. 7. Imaginary parts of the calculated πN partial-wave amplitudes [Eq. (5)] of isospin $T = 3/2$ are compared with the energy independent solutions of Ref. [33].

data can be obtained from the new hadron facilities at JPARC in Japan.

Our model is further checked by examining our predictions of the total cross sections $\sigma^{\rm tot}$ which can be calculated from the forward elastic-scattering amplitudes by using the optical theorem. The total elastic-scattering cross sections $\sigma^{\rm el}$ can be calculated from the predicted partial-wave amplitudes. With the normalization $\langle\vec{k}|\vec{k}'\rangle = \delta(\vec{k}-\vec{k}')$ used in Ref. [3], we have

$$\sigma^{\rm el}(W) = \sum_{T=1/2,3/2} \sigma_T^{\rm el}(W) \tag{40}$$

with

$$\sigma_T^{\rm el}(W) = \frac{(4\pi)^2}{k^2}\rho_{\pi N}(W) \times \sum_{JLS}\frac{(2J+1)}{2}\left|T^{TJ}_{\pi N(LS),\pi N(LS)}(k,k,W)\right|^2, \tag{41}$$

where $\rho_{\pi N}(W) = \pi k E_\pi(k) E_N(k)/W$ with k determined by $W = E_\pi(k) + E_N(k)$ and the amplitude $T^{TJ}_{L'S'(\pi N),LS(\pi N)}(k,k;W)$ is the partial-wave solution of Eq. (5). Similarly, the total $\pi N \to \eta N$ cross sections can be

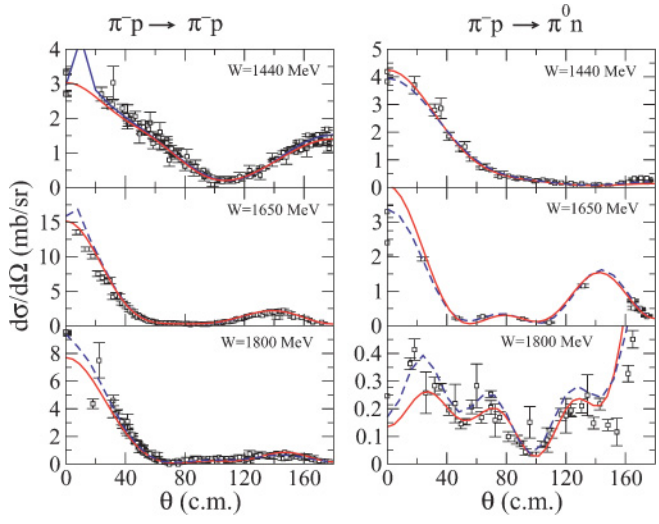

FIG. 8. (Color online) Differential cross section for several different center-of-mass energies. Solid red curve corresponds to our model, whereas blue dashed lines correspond to the SP06 solution of SAID [33]. All data have been obtained through the SAID online applications. Ref. [33].

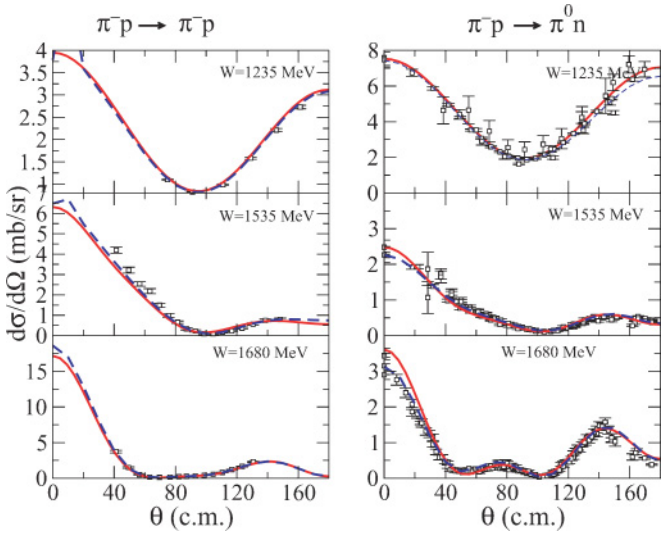

FIG. 9. (Color online) Differential cross section for several different center-of-mass energies. Similar description as for Fig. 8. All data have been obtained through the SAID online applications. Ref. [33].

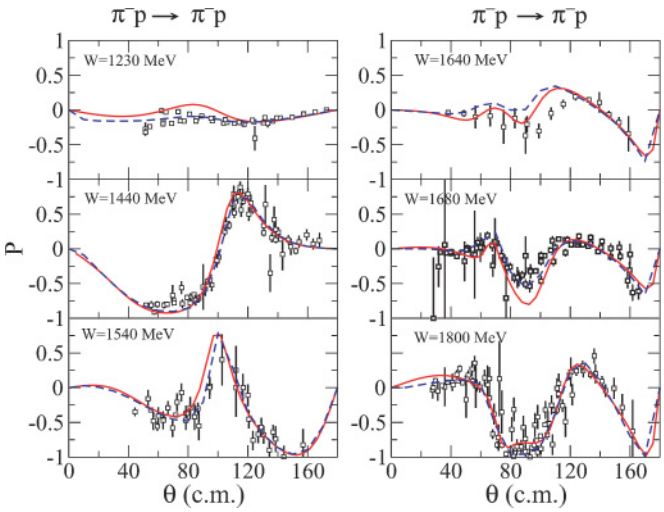

FIG. 10. (Color online) Target polarization asymmetry, P, for several different center-of-mass energies. Similar description as for Fig. 8. All data have been obtained through the SAID online applications. Ref. [33].

calculated from

$$\sigma^{\rm tot}_{\pi N\to\eta N} = \frac{(4\pi)^2}{k^2}\rho^{1/2}_{\pi N}(W)\rho^{1/2}_{\eta N}(W) \times \sum_{JLS}\frac{(2J+1)}{2}\left|T^{T=1/2,J}_{\eta N(LS),\pi N(LS)}(k',k,W)\right|^2, \quad (42)$$

where $\rho_{\eta N}(W) = \pi k' E_\eta(k') E_N(k')/W$ with k' determined by $W = E_\eta(k') + E_N(k')$. We can also calculate the contribution from each of the unstable channels, $\pi\Delta$, ρN, and σN, to the total $\pi N \to \pi\pi N$ cross sections. For example, we have for the $\pi N \to \pi\Delta \to \pi\pi N$ contribution in the center-of-mass

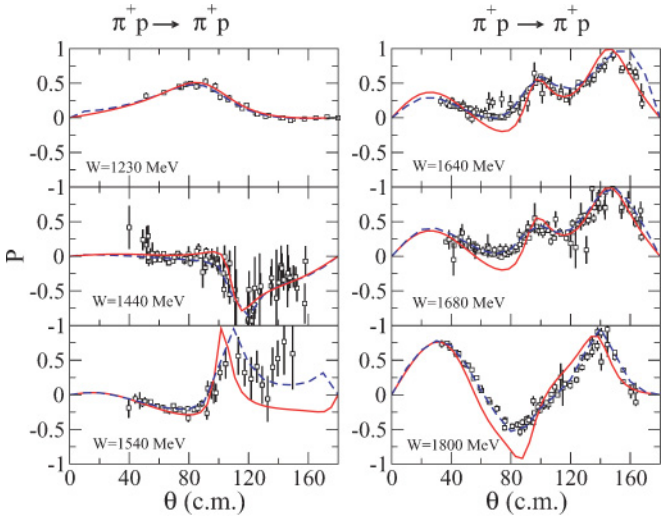

FIG. 11. (Color online) Target polarization asymmetry, P, for several different center-of-mass energies. Description as for Fig. 8. All data have been obtained through the SAID online applications. Ref. [33].

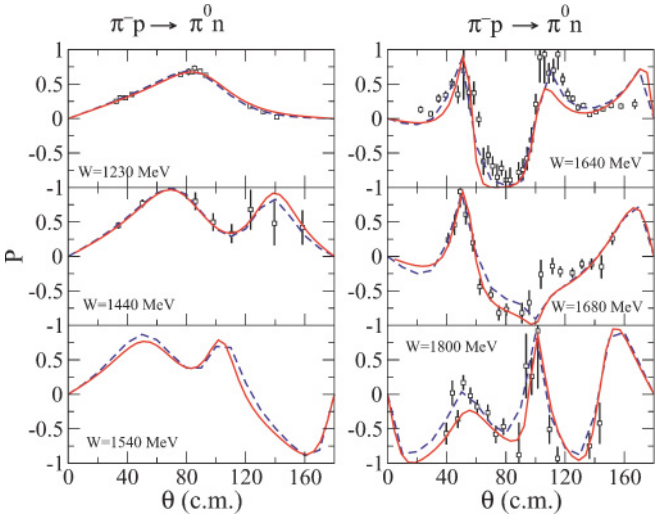

FIG. 12. (Color online) Target polarization asymmetry, P, for several different center-of-mass energies. Description as for Fig. 8. All data have been obtained through the SAID online applications. Ref. [33].

frame

$$\sigma^{\rm rec}_{\pi\Delta}(W) = \int_{m_N+m_\pi}^{W-m_\pi} dM_{\pi N}\frac{M_{\pi N}}{E_\Delta(k)} \times \frac{\Gamma_{\pi\Delta}(k,E)/(2\pi)}{|W - E_\pi(k) - E_\Delta(k) - \Sigma_{\pi\Delta}(k,E)|^2} \times \sigma_{\pi N\to\pi\Delta}(k,W), \quad (43)$$

where k is defined by $M_{\pi N} = E_\pi(k) + E_N(k)$, $E_{\pi N}(k) = [M^2_{\pi N} + k^2]^{1/2}$, $\Sigma_{\pi\Delta}(k,E)$ is defined in Eq. (19), $\Gamma_{\pi\Delta}(k,E) = -2{\rm Im}[\Sigma_{\pi\Delta}(k,E)]$, and

$$\sigma_{\pi N\to\pi\Delta}(k,W) = 4\pi\rho_{\pi N}(k_0)\rho_{\pi\Delta}(k) \times \sum_{L'S',LS,J}\frac{2J+1}{(2S_N+1)(2S_\pi+1)} \times \left|T^J_{\pi\Delta(L'S'),\pi N(LS)}(k,k_0;W)\right|^2, \quad (44)$$

where k_0 is defined by $W = E_\pi(k_0) + E_N(k_0)$ and $\rho_{ab}(k) = \pi k E_a(k) E_b(k)/W$. The amplitude $T^J_{L'S'(\pi\Delta),LS(\pi N)}(k,k_0;W)$ is the partial-wave solution of Eq. (5). The corresponding expressions for the unstable channels ρN and σN can be obtained from Eqs. (43)–(44) by changing the channel labels.

The predicted $\sigma^{\rm tot}$ (solid curves) along with the resulting total elastic-scattering cross sections $\sigma^{\rm el}$ compared with the data of $\pi^+ p$ reaction are shown in Fig. 13. Clearly, the model can account for the data very well within the experimental errors. Here only the $T = 3/2$ partial waves are relevant. Equally good agreement with the data for $\pi^- p$ reaction are shown in the left side of Fig. 14. In the right side, we show how the contributions from each channel add up to get the total cross sections.

Figure 15 shows the comparison of the contribution from the ηN channel in Fig. 14 with the data. Here we like to briefly mention how our parameters are refined by also fitting the cross-section data directly. The dashed curve in Fig. 15

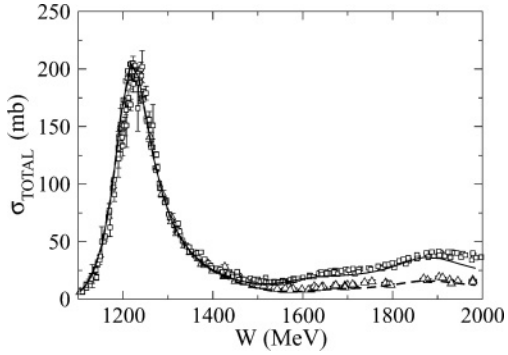

FIG. 13. The predicted total cross sections of the $\pi^+ p \to X$ (solid curve) and $\pi^+ p \to \pi^+ p$ (dashed curve) reactions are compared with the data. Squares and triangles are the corresponding data from Ref. [40].

corresponds to a preliminary result prior to the inclusion of the total cross-section data shown in Fig. 15 in the χ^2 search. To obtain the solid curve in Fig. 15, which is in a fairly good agreement with the data, we incorporated a minimal set of experimental cross-section data into the fitting procedure. By varying mainly the coupling parameter of the isospin 1/2 resonances to the ηN channel we could also get agreement with the data shown in Fig. 15, whereas retaining the very good reproduction of the πN amplitudes. Some values of such couplings to ηN channel, which were less constrained before we include the $\pi N \to \eta N$ cross section data into the analysis, can change by 50% from the χ^2 fit. Similar procedures will be needed in our further refinement of the parameters of the model by also including the data of $\pi N \to \pi\pi N$ in the χ^2 fit. Our progress in this direction will be reported elsewhere.

The contributions from $\pi\Delta$, ρN, and σN intermediate states to the $\pi^- p \to \pi\pi N$ total cross sections calculated from our model can be seen in the right side of Fig. 14. These predictions remain to be verified by the future experiments. The existing $\pi N \to \pi\pi N$ data are not sufficient for extracting

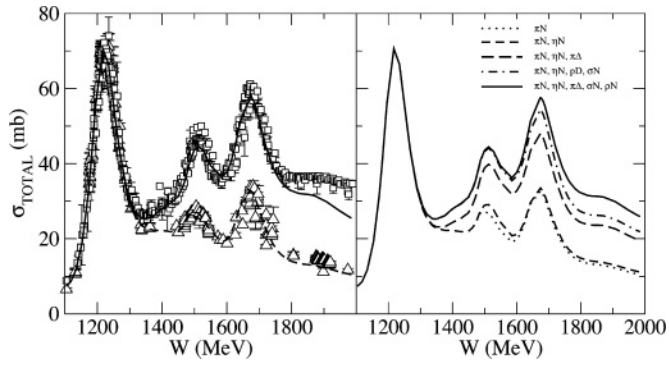

FIG. 14. (Left) The predicted total cross sections of the $\pi^- p \to X$ (solid curve) and $\pi^- p \to \pi^- p + \pi^0 n$ (dashed curve) reactions are compared with the data. Open squares are the data on $\pi^- p \to X$ from Ref. [40], open triangles are obtained by adding the $\pi^- p \to \pi^- p$ and $\pi^- p \to \pi^0 n$ data obtained from Ref. [40] and SAID database [41], respectively. (Right) Show how the predicted contributions from each channel are added up to the predicted total cross sections of the $\pi^- p \to X$.

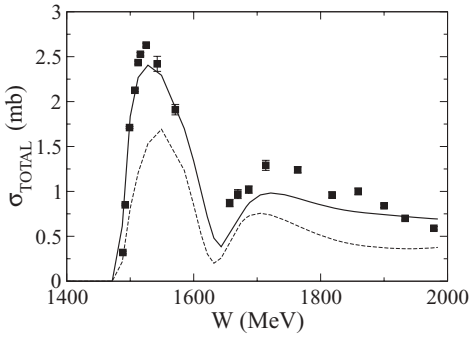

FIG. 15. The predicted total cross sections of $\pi^- p \to \eta n$ reaction, see text for details, are compared with the data [42,43].

model independently the contributions from each unstable channel. The results shown in Figs. 13–15 indicate that our parameters are consistent with the total cross-section data.

We now discuss the parameters presented in Appendix A. It is rather difficult to compare the resulting nonresonant coupling constants listed in Table III with the values from other works, because the coupling strengths are also determined by the cutoff parameters listed in Table IV. Perhaps it is possible to narrow their differences by using a different parametrization of the form factors. However, the fit is a rather time-consuming process and hence no attempt is made in this work to try other forms of form factors.

In Table V, we see that all of the bare masses are higher than the PDG's resonance positions. This can be understood from the expression Eq. (14) for the partial waves with only one N^* because one finds in general that $\mathrm{Re}[\bar{\Sigma}(E)] < 0$. For the S_{11}, P_{11}, P_{33}, and D_{13} partial waves, two bare N^* states are mixed by their interactions, as can be seen in Eq. (10). Thus the relation between their bare masses and the resonance positions identified by PDG is much more complex.

As we mentioned above, the fit to πN elastic scattering cannot determine well the bare $N^* \to \pi\Delta, \rho N, \sigma N$ parameters. Thus the results for these unstable particle channels listed in Tables III–VII must be refined by fitting the $\pi N \to \pi\pi N$ data.

VI. SUMMARY AND FUTURE DEVELOPMENTS

Within the formulation developed in Ref. [3], we have constructed a dynamical coupled-channels model of πN scattering by fitting the πN-scattering data. The parameters of the model are first determined by fitting as much as possible the empirical πN elastic scattering amplitudes of SAID up to 2 GeV. We then refine and confirm the resulting parameters by directly comparing the predicted differential cross section and target polarization asymmetry with the original data of the elastic $\pi^\pm p \to \pi^\pm p$ and charge-exchange $\pi^- p \to \pi^0 n$ processes. The predicted total cross sections of πN reactions are also in good agreement with the data. The model thus can be used as a starting point for analyzing the very extensive data of electromagnetic π production reactions.

The predicted total cross sections of $\pi N \to \eta N$ reactions are also in fair agreement with the data. However, the parameters associated with the ηN channel need to be refined to also fit the differential cross-section data of $\pi N \to \eta N$ before the model can be used to analyze the data of electromagnetic η production reactions.

The main shortcoming of this work is that the $\pi\pi N$ interaction term $h_{\pi\pi N}$ of Eq. (4) is not included in the calculations. As derived in Ref. [3], the effects due to this interaction can be included by adding a term $Z^{(I)}_{MB,M'B'}(E)$, which contains the $\pi\pi N \to \pi\pi N$ scattering amplitude, to the driving term $V_{MB,M'B'}(E)$ of Eq. (6). Our effort in this direction is in progress along with the development of a more complete determination of the parameters of the model by fitting both the data of πN elastic scattering and $\pi N \to \pi\pi N$ reactions. This is also essential to pin down the parameters of the interactions associated with the $\pi\Delta$, ρN, and σN states. Only when this second-stage is completed can we then perform dynamical coupled-channels analysis of the very extensive and complex data of photo- and electroproduction of two pions. This is an essential step to probe the $W > 1.7$ GeV resonance region where the information on N^* is very limited and uncertain.

Finally, a necessary next step is to extract the resonance poles and the associated residues from the predicted πN amplitudes. This is being pursued and will be published elsewhere [44].

ACKNOWLEDGMENTS

We thank M. Paris for his assistance in using the parallel processors at NERSC and A. Parreño for her help and encouragement to use the BSC. This work is supported by the U.S. Department of Energy, Office of Nuclear Physics Division, under contract No. DE-AC02-06CH11357 and contract No. DE-AC05-060R23177, under which Jefferson Science Associates operates Jefferson Lab, and by the Japan Society for the Promotion of Science, Grant-in-Aid for Scientific Research(c) 15540275. This work is also partially supported by grant No. FIS2005-03142 from MEC (Spain) and FEDER and European Hadron Physics Project RII3-CT-2004-506078. The computations were performed at NERSC (LBNL) and Barcelona Supercomputing Center (BSC/CNS) (Spain). The authors thankfully acknowledge the computer resources, technical expertise, and assistance provided by the Barcelona Supercomputing Center—Centro Nacional de Supercomputacion (Spain).

TABLE III. The parameters associated with the Lagrangians Eqs. (22)–(35). The results are from fitting the empirical πN partial-wave amplitudes [33] of a given total isospin $T = 1/2$ or $3/2$. The parameters from the SL model of Ref. [13] are also listed.

Parameter		SL model
$f^2_{\pi NN}/(4\pi)$	0.08	0.08
m_σ (MeV)	500.1	–
$f_{\pi N\Delta}$	2.2061	2.0490
$f_{\eta NN}$	3.8892	–
$g_{\rho NN}$	8.7214	6.1994
κ_ρ	2.654	1.8250
$g_{\omega NN}$	8.0997	10.5
κ_ω	1.0200	0.0
$g_{\sigma NN}$	6.8147	–
$g_{\rho\pi\pi}$	4.	6.1994
$f_{\pi\Delta\Delta}$	1.0000	–
$f_{\rho N\Delta}$	7.516	–
$g_{\sigma\pi\pi}$	2.353	–
$g_{\omega\pi\rho}$	6.955	–
$g_{\rho\Delta\Delta}$	3.3016	–
$k_{\rho\Delta\Delta}$	2.0000	–

APPENDIX: PARAMETERS FROM THE FITS

TABLE IV. Cutoffs of the form factors, Eq. (36), of the nonresonant interaction $v_{MB,M'B'}$. The results are from fitting the empirical πN partial-wave amplitudes [33] of a given total isospin $T = 1/2$ or $3/2$. The parameters from the SL model of Ref. [13] are also listed.

Parameter	(MeV)	SL model (MeV)
$\Lambda_{\pi NN}$	809.05	642.18
$\Lambda_{\pi N\Delta}$	829.17	648.18
$\Lambda_{\rho NN}$	1086.7	1229.1
$\Lambda_{\rho\pi\pi}$	1093.2	1229.1
$\Lambda_{\omega NN}$	1523.18	–
$\Lambda_{\eta NN}$	623.56	–
$\Lambda_{\sigma NN}$	781.16	–
$\Lambda_{\rho N\Delta}$	1200.0	–
$\Lambda_{\pi\Delta\Delta}$	600.00	–
$\Lambda_{\sigma\pi\pi}$	1200.0	–
$\Lambda_{\omega\pi\rho}$	600.00	–
$\Lambda_{\rho\Delta\Delta}$	600.00	–

TABLE V. The masses of the nucleon excited states included in the fits (second and third columns). The first column contains the masses of the nucleon resonances given by PDG [40].

L_{TJ}	PDG's mass (MeV)	M_1 (MeV)	M_2 (MeV)
S_{11}	1535; 1655	1800	1880
S_{31}	1630	1850	
P_{11}	1440; 1710	1763	2037
P_{13}	1720	1711	
P_{31}	1910	1900.3	
P_{33}	1232; 1600	1391	1602
D_{13}	1520; 1700	1899.1	1988
D_{15}	1675	1898	
D_{33}	1700	1976	
D_{35}	1960	–	
F_{15}	1685	2187	
F_{35}	1890	2162	
F_{37}	1930	2137.8	

TABLE VI. The coupling constants $C_{N^*,JTLS;MB}$ of Eq. (37) with $MB = \pi N, \eta N, \pi\Delta, \sigma N, \rho N$ for each of the resonances. When there are more than one value for $\pi\Delta$ and ρN channels, they correspond to the possible quantum numbers (LS) listed in Table II.

	πN	ηN	$\pi\Delta$		σN		ρN	
S_{11} (1)	7.0488	9.1000	−1.8526		−2.7945	2.0280	0.02736	
S_{11} (2)	9.8244	0.60000	0.04470		1.1394	−9.5179	−3.0144	
S_{31}	5.275002	–	−6.17463		–	−4.2989	5.63817	
P_{11} (1)	3.91172	2.62103	−9.90545		−7.1617	−5.1570	3.45590	
P_{11} (2)	9.9978	3.6611	−6.9517		8.62949	−2.9550	−0.9448	
P_{13}	3.2702	−0.99924	−9.9888	−5.0384	1.0147	−0.00343	1.9999	−0.08142
P_{31}	6.80277	–	2.11764		–	9.91459	0.15340	
P_{33} (1)	1.31883	–	2.03713	9.53769	–	−0.3175	1.0358	0.76619
P_{33} (2)	1.3125	–	1.0783	1.52438	–	2.0118	−1.2490	0.37930
D_{13} (1)	0.44527	−0.0174	−1.9505	.97755	−0.481855	1.1325	−0.31396	0.17900
D_{13} (2)	0.46477	0.35700	9.9191	3.8752	−5.4994	0.28916	9.6284	−.14089
D_{15}	0.31191	−0.09594	4.7920	0.01988	−0.45517	−0.17888	1.248	−0.10105
D_{33}	0.9446	–	3.9993	3.9965	–	0.16237	3.948	−.85580
F_{15}	0.06223	0.0000	1.0395	0.00454	1.5269	−1.0353	1.6065	−.0258
F_{35}	0.173934	–	−2.96090	−1.09339	–	−.07581	8.0339	−.06114
F_{37}	0.25378	–	−0.3156	−0.0226	–	0.100	0.100	0.100

TABLE VII. The range parameter $\Lambda_{N^*,JTLS;MB}$ (in units of MeV/c) of Eq. (37) with $MB = \pi N, \eta N, \pi\Delta, \sigma N, \rho N$ for each of the resonances. When there are more than one value for $\pi\Delta$ and ρN channels, they correspond to the possible quantum numbers (LS) listed in Table II.

	πN	ηN	$\pi\Delta$		σN		ρN	
S_{11} (1)	1676.4	598.97	554.04		801.03	1999.8	1893.6	
S_{11} (2)	533.48	500.02	1999.1		1849.5	796.83	500.00	
S_{31}	2000.00	–	500.00		–	500.031	500.00	
P_{11} (1)	1203.62	1654.85	729.0		1793.0	621.998	1698.90	
P_{11} (2)	646.86	897.84	501.26		1161.20	500.06	922.280	
P_{13}	1374.0	500.23	500.00	500.770	640.50	500.00	500.10	1645.2
P_{31}	828.765	–	1999.9		–	1998.8	2000.6	
P_{33} (1)	880.715	–	507.29	501.73	–	606.78	1043.4	528.37
P_{33} (2)	746.205	–	846.37	780.96	–	584.98	500.240	1369.7
D_{13} (1)	1658.	1918.2	976.36	1034.5	1315.8	599.79	1615.1	1499.50
D_{13} (2)	1094.0	678.41	1960.0	660.02	1317.0	550.14	597.57	1408.7
D_{15}	1584.7	1554.0	500.77	820.17	507.07	735.40	749.41	937.53
D_{33}	806.005	–	1359.38	608.090	–	1514.98	1998.99	956.61
F_{15}	1641.6	655.87	1899.5	522.68	500.93	500.76	500.0	1060.9
F_{35}	1035.28	–	1227.999	586.79	–	1514.3	593.84	1506.0
F_{37}	1049.04	–	1180.2	1031.81	–	600.02	600.00	600.02

[1] V. Burkert and T.-S. H. Lee, Int. J. Mod. Phys. E **13**, 1035 (2004).
[2] T.-S. H. Lee and L. C. Smith, J. Phys. G **34**, S83 (2007).
[3] A. Matsuyama, T. Sato, and T.-S. H. Lee, Phys. Rep. **439**, 193 (2007).
[4] R. Aaron, R. D. Amado, and J. E. Young, Phys. Rev. **174**, 2022 (1968).
[5] R. Aaron, D. C. Teplitz, R. D. Amado, and J. E. Young, Phys. Rev. **187**, 2047 (1969).
[6] R. Aaron and R. D. Amado, Phys. Rev. Lett. **19**, 1316 (1971); Phys. Rev. D **7**, 1544 (1973).
[7] R. Aaron and R. D. Amado, Phys. Rev. Lett. **18**, 1157 (1973).
[8] B. C. Pearce and I. R. Afnan, Phys. Rev. C **34**, 991 (1986); **40**, 220 (1989).
[9] I. R. Afnan and B. C. Pearce, Phys. Rev. C **35**, 737 (1987).
[10] I. R. Afnan, Phys. Rev. C **38**, 1792 (1988).
[11] B. C. Pearce and B. K. Jennings, Nucl. Phys. **A528**, 655 (1991).
[12] F. Gross and Y. Surya, Phys. Rev. C **47**, 703 (1993).
[13] T. Sato and T.-S. H. Lee, Phys. Rev. C **54**, 2660 (1996).
[14] T. Sato and T.-S. H. Lee, Phys. Rev. C **63**, 055201 (2001).
[15] B. Julia-Diaz, T.-S. H. Lee, T. Sato, and L. C. Smith, Phys. Rev. C **75**, 015205 (2007).
[16] C. Schutz, J. W. Durso, K. Holinde, and J. Speth, Phys. Rev. C **49**, 2671 (1994).
[17] C. Schutz, K. Holinde, J. Speth, B. C. Pearce, and J. W. Durso, Phys. Rev. C **51**, 1374 (1995).
[18] C. Schutz, J. Haidenbauer, J. Speth, and J. W. Durso, Phys. Rev. C **57**, 1464 (1998).
[19] O. Krehl, C. Hanhart, S. Krewald, and J. Speth, Phys. Rev. C **60**, 055206 (1999); **62**, 025207 (2000).
[20] A. M. Gasparyan, J. Haidenbauer, C. Hanhart, and J. Speth, Phys. Rev. C **68**, 045207 (2003).
[21] C. C. Lee, S. N. Yang, and T.-S. H. Lee, J. Phys. G **17**, L131 (1991).
[22] C. T. Hung, S. N. Yang, and T.-S. H. Lee, Phys. Rev. C **64**, 034309 (2001).
[23] V. Pascalutsa and J. A. Tjon, Phys. Rev. C **61**, 054003 (2000).
[24] A. D. Lahiff and I. R. Afnan, Phys. Rev. C **60**, 024608 (1999).
[25] A. D. Lahiff and I. R. Afnan, Phys. Rev. C **66**, 044001 (2002).
[26] M. G. Fuda and H. Alharbi, Phys. Rev. C **68**, 064002 (2003).
[27] M. Kobayashi, T. Sato, and H. Ohtsubo, Prog. Theor. Phys. **98**, 927 (1997).
[28] T.-S. H. Lee and A. Matsuyama, Phys. Rev. C **32**, 516 (1985).
[29] Herman Feshbach, *Theoretical Nuclear Physics, Nuclear Reactions* (Wiley, New York, 1992).
[30] A. W. Thomas (ed.), *Topics in Current Physics: Modern Three-Hadron Physics* (Springer-Verlag, Berlin, 1977).
[31] As reviewed by H. Garcilazo and H. Mizutani, $\pi - NN$ *System* (World Scientific, Singapore, 1990).
[32] J. A. Johnstone and T.-S. H. Lee, Phys. Rev. C **34**, 243 (1986).
[33] R. A. Arndt, I. I. Strakovsky, and R. L. Workman, Phys. Rev. C **53**, 430 (1996); Int. J. Mod. Phys. A **18**, 449 (2003).
[34] See, for example, R. B. Wiringa, V. G. J. Stoks, and R. Schiavilla, Phys. Rev. C **51**, 38 (1995).
[35] The Lorentz boost factors for transforming the matrix elements of $\Delta \to \pi N$ $(\rho, \sigma \to \pi\pi)$ vertex interaction from the πN $(\pi\pi)$ to the $\pi\pi N$ center-of-mass frames, which were not given in Ref. [3], are included here.
[36] J. D. Bjorken and S. D. Drell, *Relativistic Quantum Field Theory* (McGraw-Hill, New York, 1964).
[37] A. Matsuyama, Phys. Lett. **B152**, 42 (1984).
[38] A. Matsuyama and T.-S. H. Lee, Phys. Rev. C **34**, 1900 (1986).
[39] K. Nakayama, Y. Oh, J. Haidenbauer, and T.-S. H. Lee, Phys. Lett. **B648**, 351 (2007).
[40] W. M. Yao *et al*. (Particle Data Group), J. Phys. G **33**, 1 (2006).
[41] CNS Data Analysis Center, GWU, http://gwdac.phys.gwu.edu.
[42] S. Prakhov *et al*., Phys. Rev. C **72**, 015203 (2005).
[43] Robert M. Brown *et al*., Nucl. Phys. **B153**, 89 (1979).
[44] N. Suzuki, T. Sato, and T.-S. H. Lee (in preparation).